Journal of Molecular Catalysis A: Chemical 323 (2010) 45–51

Contents lists available at ScienceDirect

Journal of Molecular Catalysis A: Chemical

journal homepage: www.elsevier.com/locate/molcata

SBA-15 as support for NiMo HDS catalysts derived from sulfur-containing molybdenum and nickel complexes: Effect of activation mode

Z.D. Huang[a], W. Bensch[a,*], A. Lotnyk[b], L. Kienle[b], S. Fuentes[c], J. Bocarando[d], G. Alonso[c], C. Ornelas[d]

[a] Institut für Anorganische Chemie, University of Kiel, Max-Eyth-Str. 2, D-24118 Kiel, Germany
[b] Faculty of Engineering, Institute for Material Science, Synthesis and Real Structure, Christian Albrechts University of Kiel, Kaiserstr. 2, D-24143 Kiel, Germany
[c] Universidad Nacional Autónoma de México, Centro de Nanociencias y Nanotecnología, Ensenada, B.C., C.P. 22860, México
[d] Centro de Investigación en Materiales Avanzados S. C., Chihuahua, Chih., C.P. 31109, Mexico

ARTICLE INFO

Article history:
Received 7 July 2009
Received in revised form 4 March 2010
Accepted 7 March 2010
Available online 12 March 2010

Keywords:
Hydrodesulfurization
NiMo/SBA-15 catalysts
TEM
In situ activation
Ex situ activation

ABSTRACT

Ex situ and *in situ* decomposition of the sulfur-containing precursors ammonium thiomolybdate (ATM) and nickel diethyldithiocarbamate (NiDETC) was applied for the preparation of SBA-15-supported NiMo catalysts. The catalysts were characterized with X-ray diffraction (XRD), N_2-physisorption and high-resolution transmission electron microscopy (HRTEM). The *in situ* activation performed in the presence of hydrocarbon solvent during the HDS of dibenzothiophene is more beneficial for the preparation of NiMo catalysts with a high HDS performance compared to the *ex situ* activation mode using a N_2/H_2 (10% H_2) gas flow at 773 K. Low MoS_2 stacking, small MoS_2 slabs and a less pronounced pore blocking present in the *in situ* activated NiMo/SBA-15 materials might be mainly responsible for the high HDS performance. In addition, the *in situ* decomposition mode is a "softer" reducing atmosphere and represents a beneficial condition for the generation of the catalytic active "NiMoS" phase.

1. Introduction

In many countries new and severe environmental regulations concerning the reduction of sulfur in gasoline and in automotive diesel fuel require the development of more effective hydrodesulfurization (HDS) catalysts. The final goals in the European Union are 10 ppm sulfur automotive diesel, reduction of the sulfur content in so-called off-road diesel from 1000 to 10 ppm for land-based uses and to 300 ppm for inland waterway engines. The usage of high-performance HDS catalysts is the most economical way to achieve these low sulfur concentration levels. Hence, a large number of synthetic approaches were applied to reach this final goal. Industrial catalysts are normally prepared via an oxidic route, i.e., the support material like γ-Al_2O_3 is wet impregnated with Mo heptamolybdate and suitable Ni/Co salts [1]. In this step of preparation the catalysts are present as finely dispersed oxides and different procedures are applied for the conversion of the oxides into the sulfides. The most common procedures are the *ex situ* and the *in situ* presulfiding approaches. In the former process the activation of the catalyst is done in two steps, i.e., the oxides are first impregnated with an S containing compound leading to not fully sulfided catalysts. In the second step, the catalysts are loaded in the reactor where the H_2 is supplied for the activation of the catalyst. A different *ex situ* procedure is also applied where the conversion from the oxides to the sulfides and also the activation are performed outside the reactor system.

For *in situ* processing the oxidic catalyst is loaded in the reactor system and treated at high temperature and high pressure with H_2 and the sulfur containing feed [[1] and references therein]. Besides the oxidic route several other synthetic procedures were applied like the thermal decomposition of suitable molecular complexes as precursors [2], the usage of ammonium thiomolybdates/thiotungstates [3–9], or applying chelating ligands [10–12]. An overview about synthesis strategies, activation procedures and selection of suitable supports was recently published [13]. We recently introduced a new preparation method which may be called all-sulfide route [14]. The main characteristics of this approach are the application of suitable sulfidic precursors like ammonium thiomolybdate (ATM) and Ni or Co thiocarbamate. The resulting materials must not be sulfided in H_2S or an S containing organic solvent but are rather obtained by thermal decomposition in H_2/N_2 atmosphere.

Besides the variation of the synthesis procedures the influence of the support material was also studied using TiO_2, $MgO–Al_2O_3$, ZrO_2, carbon and so on. Recently, mesoporous SBA-15 has been employed as HDS catalyst support due the large specific surface area and especially a relatively high thermal stability, being superior to other silica molecular sieves such as HMS and MCM-41 [15–20].

* Corresponding author. Tel.: +49 431 880 2406; fax: +49 431 880 1520.
E-mail address: wbensch@ac.uni-kiel.de (W. Bensch).

1381-1169/$ – see front matter © 2010 Elsevier B.V. All rights reserved.
doi:10.1016/j.molcata.2010.03.009

More recently, ammonium thiomolybdate (ATM) and carbon-containing ammonium thiomolybdate compounds have been used as precursors by us [14,21,22] to prepare (Ni)CoMo sulfide catalysts supported on mesoporous SBA-15. Interestingly, higher HDS activity compared to a commercial HDS catalyst supported on γ-Al_2O_3 material was observed despite the presence of large MoS_2 stacking. High-resolution transmission electron microscopy investigations showed a high density of imperfect/disordered MoS_2 nanocrystallites which may contain a large number of coordinatively unsaturated sites being responsible for the relatively high HDS activity.

In the present work, the effect of activation mode on the SBA-15-supported NiMo sulfide HDS catalysts will be explored. The catalysts were synthesized by thermal decomposition of sulfur-containing molybdenum (ammonium thiomolybdate, ATM) and nickel complexes (nickel diethylthiocarbamate, NiDETC) during the catalytic test (*in situ* activation) or under H_2/N_2 gas flow (*ex situ* activation). X-ray diffractometry (XRD), nitrogen physisorption using the Brunauer, Emmett and Teller (BET) method and high-resolution transmission electron microscopy (HRTEM) have been used for the investigation of the obtained supported catalysts.

2. Experimental

2.1. Sample preparation

2.1.1. Synthesis of Ni–MoS_2/SBA-15

The support material SBA-15 was prepared following the synthesis route published in Refs. [23–25]. Typically, 2 g of SBA-15 was stirred for 4 h in 100 mL saturated chloroform solution of nickel diethyldithiocarbamate (NiDETC). Afterwards, the solvent was removed by filtration and the obtained products NiDETC/SBA-15 were dried under vacuum over night. The dried product was then stirred in 150 mL saturated aqueous solutions of ammonium thiomolybdate (ATM) at 298 K. After 4 h stirring the products were filtered without washing and then activated during the catalytic test (*in situ*) or under a H_2/N_2 (H_2 = 10%) gas flow at 773 K. The catalysts are named according to the activation mode employed as, e.g., NiMo/SBA-15(iA) and NiMo/SBA-15(eA) meaning the catalysts were *in situ* or *ex situ* activated respectively. The *in situ* activated catalyst NiMo/SBA-15(iA) was obtained by placing the proper amount of the precursor material (NiDETC/ATM/SBA-15) in the reactor to give 1.0 g of the catalyst. The catalyst is obtained by the *in situ* decomposition of the precursors during the HDS test of DBT. The DBT test solution was a mixture of 6.6 g DBT in 150 mL decalin, i.e., the DBT concentration is 0.238 mol L^{-1}. In the case of NiMo/SBA-15(eA), the precursor (NiDETC/ATM/SBA-15) is decomposed by heating in a tubular furnace for 2 h under a H_2/N_2 (H_2 = 10%) gas flow at 773 K. The *ex situ* activated catalyst was then transferred to the reactor within a very short time (less than a couple of minutes) preventing oxidation of the material. The metal based composition of the catalysts was 10 wt% of Mo and 1.5 wt% of Ni. The precursor ATM was synthesized according to the synthesis method described previously [26] and the preparation of NiDETC has been reported by Cambi et al. [27].

2.2. Sample characterization

2.2.1. X-ray powder diffraction, BET and EDS analyses

X-ray diffraction (XRD) patterns were collected on a Siemens D5000 diffractometer at room temperature using monochromatized CuKα radiation (λ = 1.54056 Å). For the calculation of the sizes of the coherent scattering domains instrumental broadening was not considered. The estimated particle sizes are then by about 5–10% too small. Nitrogen adsorption measurements were carried out at 77 K on a Quantachrom Autosorb-1. Samples were degassed under flowing argon at 473 K for 2 h before nitrogen adsorption. The BET surface areas were calculated from p/p_0 = 0.03–0.3 in the adsorption branch. The chemical composition of the catalysts (in wt%, average of five measurements at different points of the sample) was determined by energy dispersive X-ray spectroscopy (EDS) analysis with a Philips ESEM XL 30 microscope.

2.2.2. Transmission electron microscopy

Transmission electron microscopy (TEM) investigations were performed with a Tecnai 30 STwin microscope (300 kV, FEG cathode, C_S = 1.2 mm). The samples for TEM investigations were prepared as follows. Small amounts of powders containing either NiMo/SBA-15(iA) or NiMo/SBA-15(eA) were suspended in methanol and ultrasonically grinded for 15 min. Afterwards, the suspended powders were transferred to a lacey carbon film fixed on a 200 mesh cooper grid by dipping of such TEM support into the solution. The prepared TEM samples were dried carefully at a room temperature. All images were recorded with a Gatan Multiscan CCD camera (2k × 2k) and evaluated (including Fourier analyses) with the program Digital Micrograph (Gatan). EDS analyses were performed in the TEM mode with a Si/Li detector (EDAX System).

2.2.3. HDS test reaction

HDS of DBT was carried out in a Parr model 4522 high-pressure batch reactor. 1.0 g of the catalyst and 150 mL of the freshly prepared solution of DBT in decalin (5%, w/w, $[DBT]_0$ = 0.2388 mol/L) were introduced in the reactor. The reactor was then purged and pressurized to 3.4 MPa (490 psi) with hydrogen and then heated up to 623 K at a rate of 10 K/min and continuous stirring of 600 rpm. After reaching the working temperature, the reaction products were collected for chromatographic analysis every half an hour to determine the conversion-time dependence during 5 h. After the reaction, the used catalysts were filtered, washed and stored in inert atmosphere. The reaction products were analyzed using a Perkin-Elmer Auto-system chromatograph with a 9 ft long × 1/8 in. diameter packed column containing chromosorb W-AW 80/100 mesh 3% OV-17 (phenyl methyl silicone 50% phenyl) as a separating phase.

The hydrodesulfurization (HDS) of dibenzothiophene (DBT) occurs by two parallel reactions pathways [28]: (I) direct desulfurization (DDS) via C–S bond cleavage and (II) hydrogenation (HYD). The main products are biphenyl (BP, via DDS), cyclohexylbenzene (CHB, via HYD) and tetrahydrodibenzothiophene (TH-DBT, via HYD). The ratio between HYD and DDS can be approximated in terms of the experimental selectivity according to the following equation:

$$\frac{\text{HYD}}{\text{DDS}} = \frac{[\text{PCH}] + [\text{TH-DBT}]}{[\text{BP}]}$$

The rate constant was determined from the DBT conversion as function of time assuming that DBT conversion being a pseudo-zero-order reaction [29] by using of following equation:

$$X_{\text{DBT}} = \frac{1 - \eta_{\text{DBT}}}{\eta_{\text{DBT}}} = \left(\frac{k}{\eta_{\text{DBT},0}}\right) t \quad (1)$$

where X_{DBT} is the fraction conversion of DBT, η_{DBT} is the moles of DBT, k is the pseudo-zero-order rate constant, t is the time in seconds and $k/\eta_{\text{DBT},0}$ is the slope. The mean standard deviation for catalytic measurements was ca. 2.5%.

Table 1
Specific surface area, normalized surface area of SBA-15 support and SBA-15-supported Ni–Mo sulfide catalysts, the mean MoS_2 crystal size and the C/Mo ratios. Normalized $(X) = X_{NiMo}/((1-y)X_{SBA-15})$, where X is the specific surface area, y is the weight fraction of NiMo sulfides.

Catalysts	Mo (wt.%)	Ni (wt.%)	BET surface area ($m^2\ g^{-1}$)		MoS_2 mean crystal size (nm)	Elemental analysis C/Mo
				Normalized		
SBA-15	0	0	742.2	1	–	–
NiMo/SBA-15(eA)	10	1.5	314.7	0.55	3.8	0.36
NiMo/SBA-15(iA)	10	1.5	491.5	0.85	2.1	2.47

3. Results

3.1. Structural characteristics of NiMo/SBA-15 catalysts

Nitrogen adsorption–desorption isotherms of the parent SBA-15 and SBA-15-supported NiMo sulfide catalysts are shown in Fig. 1. Very typical adsorption–desorption hysteresis (type-H1 hysteresis loops), characteristic for SBA-15 with cylindrical pore channels [23] is clearly observed for all samples. The isotherms of the SBA-15-supported NiMo sulfide catalysts (Fig. 1) keep the characteristic shape of the isotherm of the SBA-15 indicating that incorporation of NiMo sulfide phases and the thermal treatment during the catalytic test and under H_2/N_2 gas flow at 773 K do not affect the original pore structure of the parent material. But the NiMo sulfide incorporation reduces significantly the specific surface area determined from BET equation (Table 1). This could be explained by the dilution of the support by the supported Mo and Ni sulfide phases and the possibility of some pore blocking (see isotherms in Fig. 1). Taking into account the dilution effect of the metal loading, the normalized surface areas were calculated as described in Ref. [30]. Interestingly, the *in situ* activated NiMo/SBA-15(iA) exhibits a high normalized surface area of about 0.85 suggesting the presence of less pronounced pore blocking (Table 1).

The presence of the mesoporous structure of SBA-15 after incorporation of Mo and Ni is also evident from the XRD patterns collected at low diffraction angles (Fig. 2). The samples display three diffraction peaks associated with p6mm hexagonal symmetry suggesting that the hexagonal structure of the SBA-15 sample was maintained which is in line with the results obtained from N_2-physisorption measurements. The NiMo sulfide incorporation leads to a decrease of the reflection intensities which is caused by the strong absorption of X-rays by Mo(Ni). In addition, a partial perturbation of the long-range periodicity order of the mesoporous structure cannot be excluded [19], which also results in a reduction of the reflection intensities.

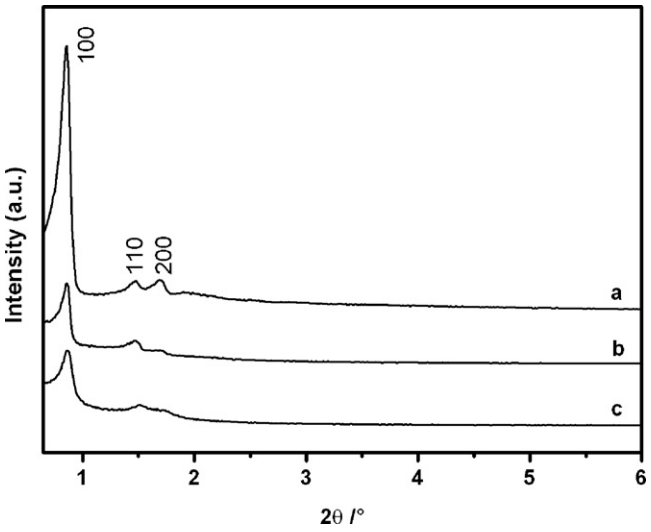

Fig. 2. XRD patterns of (a) parent SBA-15, (b) NiMo/SBA-15(iA) and (c) NiMo/SBA-15(eA).

The wide-angle XRD patterns are depicted in Fig. 3. The reflections are broad indicating the presence of poor crystalline 2H-MoS_2 and amorphous SBA-15 silica (modulation at about 22° 2θ). Apparently, the activation mode strongly affects the MoS_2 dispersion and orientation of the particles as can be seen from the different intensities of the reflections. The maximum of the (0 0 2) reflection of the samples is located at about 14.1 (eA) and 13.9° 2θ (iA) representing a shift to lower scattering angles compared to well crystalline MoS_2 (14.4° 2θ). This observation is typical for bent MoS_2 slabs introducing an expansion of the inter-layer separation [31]. The widths of the (1 0 0)/(1 0 1) reflections represent the lengths of the MoS_2 slabs. The estimated average sizes of coherent scattering MoS_2 particle sizes calculated from the (0 0 2) reflection

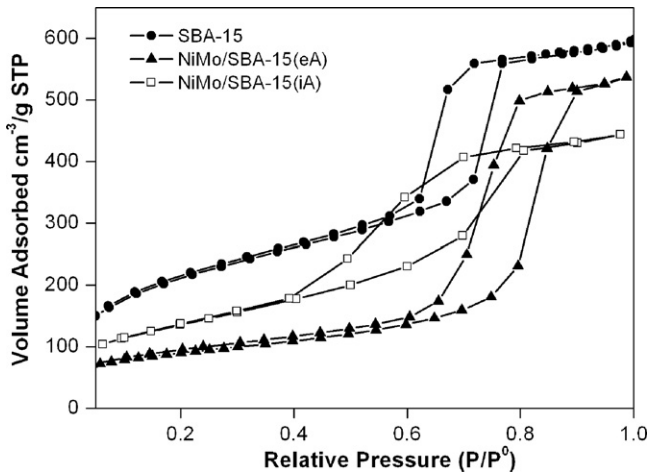

Fig. 1. Nitrogen adsorption–desorption isotherms of SBA-15 support, NiMo/SBA-15(eA) and NiMo/SBA-15(iA).

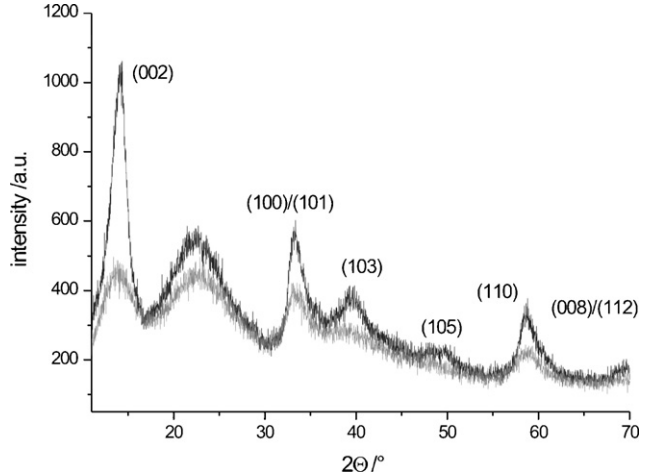

Fig. 3. Wide-angle XRD patterns of NiMo/SBA-15(eA) (black) and (b) NiMo/SBA-15(iA) (grey).

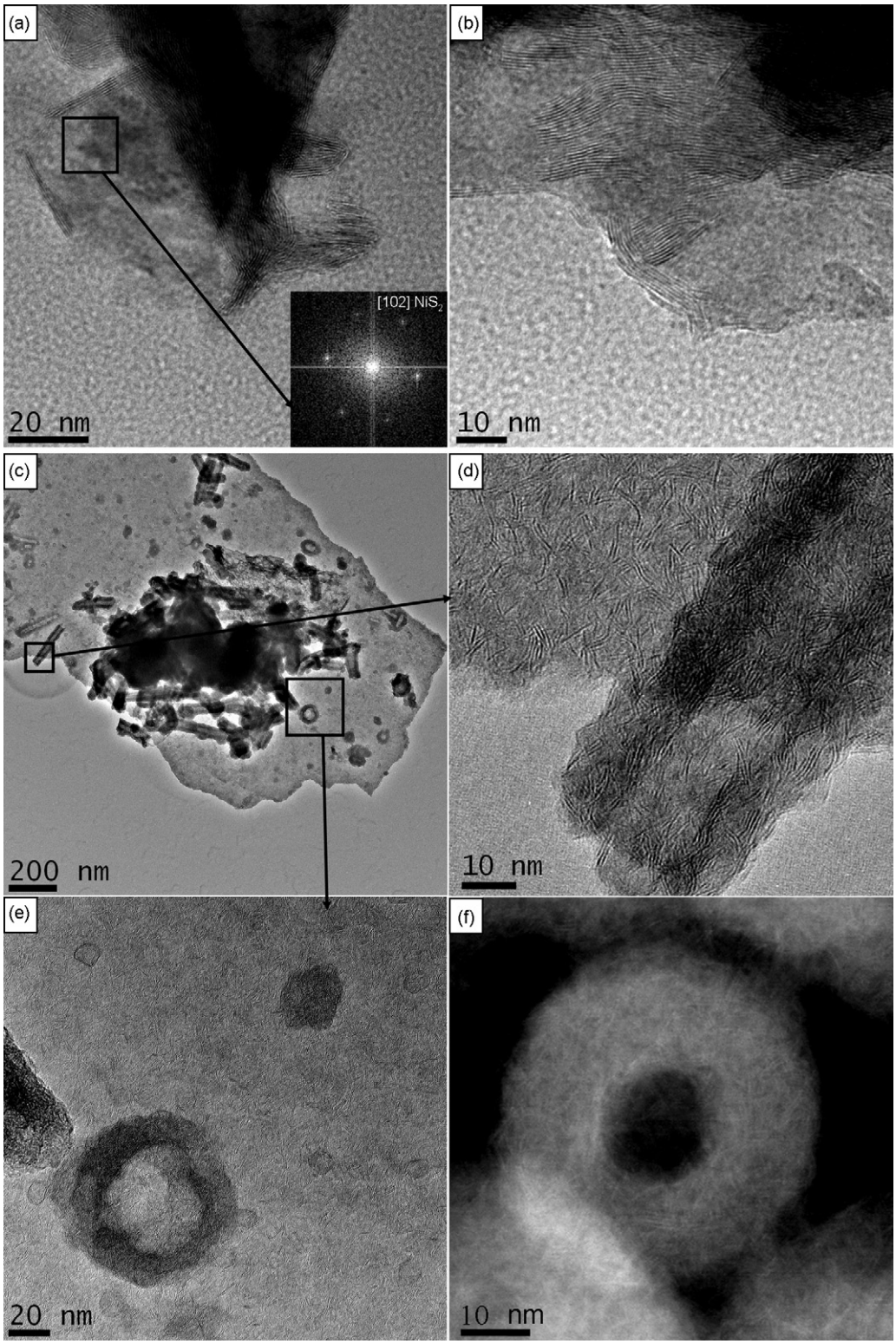

Fig. 4. TEM images of *ex situ* (a and b) and *in situ* (c to f) activated catalysts.

applying the Scherrer formula are shown in Table 1. The values of about 3.6 (eA) and 2.4 nm (iA) are considerably smaller than the pore size of SBA-15 of about 6 nm. These values indicate that the catalysts consist of only a few stacked MoS_2 slabs, i.e., about 6 MoS_2 layers in the *ex situ* activated and about 4 slabs in the *in situ* activated material. The length of the MoS_2 slabs is about 3.5 nm in both catalysts. The differences of the intensity ratios in the two powder patterns are remarkable. For the *in situ* activated material the strong depression of the (0 0 2)/(0 0 8) reflections and the absence of the (1 0 3)/(1 0 5) peaks indicate a very poor crystallinity of the material. No reflections of Ni sulfides occur in the powder pattern suggesting a very good dispersion of the promoter atoms.

The TEM images of the *ex situ* activated catalyst (Fig. 4a and b) mainly show bent MoS_2 slabs with a stacking between 3 and 10 layers with an average around 6–7 layers. Many of the nanocrystals

exhibit different types of defects like folding of the layers, stacking faults and rounded edges.

Some crystalline particles consisting mainly of Ni and S (see Fig. 4 a, rectangular area and SAED pattern) were found besides MoS_2 nanocrystals. The phase NiS_2 was identified by FFT of the highlighted area of Fig. 4a. The small size of such NiS enriched particles prevents detection in X-ray scattering experiments. The morphology of the *in situ* activated catalyst particles is totally different (Fig. 4c–f). The slabs of *in situ* activated Ni–MoS_2 (Fig. 4f) are shorter and the stacking of the MoS_2 slabs is less pronounced compared to *ex situ* activated Ni–MoS_2.

Besides some randomly arranged MoS_2 nanoslabs with very low stacking numbers (1–4) nanorings, nanotubes and nanospheres can be identified. It should be noted that typical MoS_2 flanges made of parallel MoS_2 layers are not observed in the TEM image of the nanoring shown in Fig. 4e, but nano-MoS_2 slabs with random arrangement. Anyhow, the nanoring-like structure of such aggregate of nanoslabs is recognizable in the TEM image. The diameter of the ring in the range of nanometer scale, and there is a hole in the middle of the ring. The nanoring-like structure is more visible in the HAADF-STEM image taken from another location of the TEM sample. The interpretation of HAADF-STEM images is commonly straightforward since the atom columns with the higher atomic number (Z) always shows a higher intensity compared to the atom columns with the lower Z number. Thus, the MoS_2 slabs in Fig. 4f are appearing with very bright contrast. There is also a dark area in the middle of the ring coming most probably from a light element like carbon since we used a carbon covered Cu grid for TEM investigations. Similar observation were made for the MoS_2 nanotube-like structure seen in Fig. 4 from HAADF-STEM image (not shown), i.e., the structure is not built from parallel MoS_2 layers, but is based on an aggregate of MoS_2 nanoslabs.

All these MoS_2 based nanoparticles in Fig. 4c–f contain Ni as evidenced by EDX analyses (not shown). Moreover, the EDX analysis gives evidences that the nanorods are composed of Mo, S, Ni and a relatively large amount of carbon. In addition the particles contain a larger number of different defects compared to the *ex situ* activated material. The different morphologies and the differing defect densities of the two catalysts can explain the differences seen in the X-ray powder patterns (see above).

It should be also noted that for obtaining average cluster size and stacking number of MoS_2 we recorded around ten TEM images for each sample. The images were collected from different places of a TEM sample. Up to seven MoS_2 clusters (see Fig. 4a and b) were found in each TEM image for *ex situ* activated MoS_2. These clusters were counted for obtaining an estimate about the average cluster size and stacking number. On the over hand, several hundreds of MoS_2 clusters were observed in each TEM image for *in situ* activated catalyst (see for e.g., enlarged part of Fig. 4c). Since there were no big differences between the images, we used one TEM image for the estimation of average cluster size and stacking number.

3.2. Catalytic behavior of NiMo/SBA-15 catalysts

Fig. 5 illustrates the catalytic behavior of the NiMo/SBA-15 catalysts at 623 K for HDS of DBT. The approximate linear relationship of DBT conversion with reaction time confirms the pseudo-zero-order of the reaction under the experimental conditions employed. The slight deviation from linearity appears at the end of the reaction and is associated with the deactivation of the catalyst by H_2S accumulated in the reactor [32]. Table 2 shows the initial rate constants determined by a linear fit of the experimental data according to above-described Eq. (1). Apparently, the *in situ* activation mode is more efficient in achieving active HDS catalysts than the *ex situ* preparation. In contrast to the *ex situ* activated NiMo/SBA-15(eA) catalysts ($k = 8.1 \times 10^{-7}$ mol s^{-1} g^{-1}),

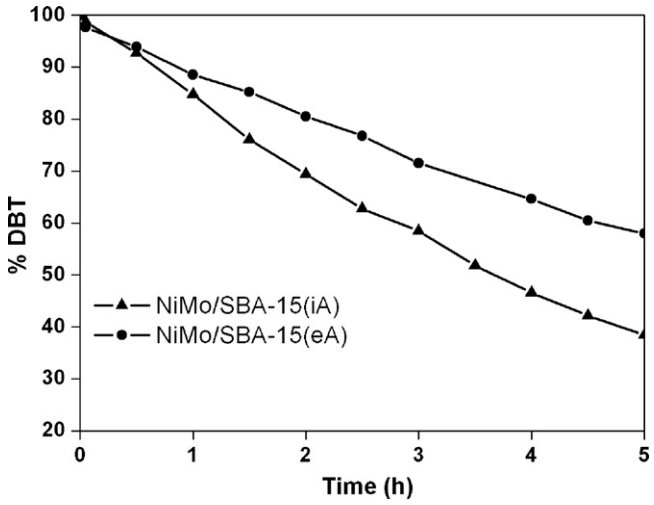

Fig. 5. Dibenzothiophene conversion as function of reaction time for the NiMo/SBA-15 catalysts.

Table 2
Initial rate constants (k) and selectivity HYD/DDS (achieved at a DBT conversion of ca. 30%) of the NiMo/SBA-15 catalysts during the HDS reaction of DBT (T = 623 K, P = 3.4 MPa).

Catalysts	k (specific) (1×10^{-7} mol s^{-1} g^{-1})	HYD/DDS ratio
NiMo/SBA-15(eA)	8.1	0.79
NiMo/SBA-15(iA)	12.8	0.84
NiMo/Al_2O_3[a]	12.0	0.53

[a] The sample is from Ref. [32].

the *in situ* activated NiMo/SBA-15(iA) represents a higher rate constant $k = 12.8 \times 10^{-7}$ mol s^{-1} g^{-1}. We note that the catalytic activity is slightly higher than the activity obtained for an industrial NiMo/Al_2O_3 catalyst characterized under the actual experimental condition. The selectivity expressed as HYD/DDS is however almost not affected by the activation mode (Table 2). The two catalysts show a slightly higher selectivity for the DDS pathway at a DBT conversion of ca. 30% (HYD/DDS = ca. 0.8).

4. Discussion

The *in situ* activation of ammonium thiometallates and carbon-containing ammonium thiometallates has been applied for the generation of unsupported cobalt promoted MoS_2 catalysts by Alonso et al. [4,7]. *In situ* activation of alkylammonium thiometallates resulted in a considerable enhancement of the specific surface areas, total pore volume and consequently the HDS activity of the final catalysts. The *in situ* activation mode was reported to be more beneficial for the preparation of active HDS catalysts using carbon-containing ammonium thiomolybdate complexes, whereas the *ex situ* activation approach is more efficient when the carbon-free ATM is employed.

The present samples display a different behavior: the *in situ* activated MoNi/SBA-15(iA) catalyst derived from ATM exhibits a higher HDS performance compared to the catalyst obtained from *ex situ* decomposition of ATM. The HDS property of the *in situ* activated catalyst is comparable with that of a commercial NiMo/Al_2O_3. The partial blocking of the pore entrances leads to a decrease in accessibility of the reactants to the active sites [33,34]. The lower pore-blockage observed for the NiMo/SBA-15(iA) catalyst using the *in situ* activation mode should have a positive effect on the catalytic activity resulting in an improved HDS activity of DBT. Another possible explanation may be the specific role of the hydrocarbon solvent applied during the *in situ* activation procedure. It is well

recognized that hydrocarbons can play the role of less tough reducing agents than H_2 during the activation of hydrotreating catalysts [7,35]. Under such "softer" reducing atmosphere, the generation of catalytic low active nickel sulfide phase Ni_3S_2 is less favored compared to the formation of the so-called active "NiMoS" phase [36], in which Ni represents a square-pyramidal-like structure as in the case of CoMo sulfide catalysts. Indeed, Ni_3S_2 aggregates more rapidly than Co_9S_8 because of its lower Tamman temperature (686 K for Co_9S_8 versus 532 K for Ni_3S_2) [37]. Therefore, the preparation of nickel promoted MoS_2 catalysts is more sensitive to the activation condition than the preparation of Co promoted MoS_2 catalysts. Moreover, the higher activity of the *in situ* activated MoNi/SBA-15 catalyst may be caused by the positive carbon effect. Indeed, the *in situ* activated sample contained a large amount of carbon (C/Mo = 2.47). The beneficial role of carbon in hydrotreating applications was discussed in Refs. [38,39], and according to these authors the main effects are: (i) a geometrical effect, i.e., a carbonaceous deposit may isolate and stabilize the active sulfide phase resulting in more dispersed MoS_2 particles; (ii) a support effect, i.e., carbon species may be deposited between the support and the sulfide phase reducing the interaction of the active phase with the support; (iii) a chemical effect leading to the formation of more active "CoMoC" phases with surface carbide-like moieties.

The main results obtained from XRD and TEM experiments give evidence that the two activation procedures lead to very different morphologies, particle sizes and Ni distribution. All these properties of the catalysts may help to explain the different catalytic activities. The catalytically active particles of the *in situ* activated material exhibit a lower stacking of the MoS_2 slabs and strongly distorted nanorings, nanotubes and nanospheres. The promoter atoms are distributed over all these particles. In contrast, a relatively large MoS_2 slab stacking is found for the *ex situ* activated material containing some amount of a NiS phase besides the Ni promoted MoS_2 material. The short slabs, low stacking, large defect density and good dispersion of the promoter atoms lead to the higher catalytic activity of the *in situ* activated material.

Selectivity results reveal that Ni promotion slightly favors the DDS pathway for the HDS of DBT not depending on the activation mode. Similar HYD/DDS ratios due to nickel promotion effects were also demonstrated by Alonso et al. for NiMo sulfide catalysts [40]. For NiMo/SBA-15(iA), the HYD activity is slightly higher compared to the catalyst using *ex situ* decomposition mode (Table 2, 0.84 versus 0.79). This phenomenon could be related to the morphology change of the actives phases. According to the rim-edge model proposed by Daage and Chianelli [41], "rim" sites at the exterior of the stacked layers would be responsible for both C–S bond breaking and hydrogenation whereas "edge" sites located on internal stacked layers is only active for C–S bond breaking reactions. Lower MoS_2 stacking present in the *in situ* activated catalyst will have the advantage of making more rim sites available for the hydrogenation reaction [32], thus resulting in the increase of the rate of the HYD pathway. However, it should be emphasized that the rim-edge model was proposed for unsupported MoS_2 catalysts and the extension of this selectivity/stacking correlation to supported NiMo sulfided catalysts has still to be done.

5. Conclusions

In the present study, the effect of the decomposition mode on nickel promoted MoS_2 supported on SBA-15 derived from sulfur-containing molybdenum (ATM) and nickel complexes (NiDETC) was investigated. The *in situ* activation mode generates a NiMo/SBA-15 catalyst with higher HDS performance compared to the one prepared from *ex situ* decomposition under H_2/N_2 atmosphere. Several possible explanations for the good HDS properties can be given. (1) High MoS_2 dispersion with low MoS_2 stacking is found for the *in situ* activated catalyst (XRD, TEM). Furthermore, the MoS_2 nanocrystallites exhibit different morphologies with many different defects. Some of the morphologies like the nanotubes may be formed due to the presence of large amounts of carbon. One identifiable effect of carbon is of geometrical nature, but other possible carbon effects such as a chemical effect (formation of carbide-like compounds) and a support effect cannot be excluded. (2) The synergetic effect of nickel depends on the mode of activation. The *in situ* mode of decomposition, a "softer" reducing atmosphere, is shown to be a beneficial condition for generation of the catalytic active "NiMoS" phase. (3) A larger pore-blockage was observed for the *ex situ* activated catalysts. The blocking of the pores may lead to reduced accessibility of the reactants to the active sites yielding a lower catalytic activity.

Acknowledgements

The financial support of the Deutsche Forschungsgemeinschaft (DFG, BE 1653/17-1) and of the State of Schleswig-Holstein is greatly acknowledged. The authors are thankful to Ms. Szillus for TEM sample preparation.

References

[1] S. Eijsbouts, A.A. Battiston, G.C. van Leerdam, Catal. Today 130 (2008) 361.
[2] T.C. Ho, Catal. Today 130 (2008) 206.
[3] K. Wilkinson, M.D. Merchan, P.T. Vasudevan, J. Catal. 171 (1997) 325.
[4] H. Nava, C. Ornelas, A. Aguilar, G. Berhault, S. Fuentes, G. Alonso, Catal. Lett. 86 (2003) 257.
[5] G. Alonso, M. Del Valle, J. Cruz, V. Petranovskii, A. Licea-Claverie, S. Fuentes, Catal. Today 43 (1998) 117.
[6] G. Alonso, G. Berhault, A. Aguilar, V. Collins, C. Ornelas, S. Fuentes, R.R. Chianelli, J. Catal. 208 (2002) 359.
[7] L. Alvarez, J. Espino, C. Ornelas, J.L. Rico, M.T. Cortez, G. Berhault, G. Alonso, J. Mol. Catal. A: Chem. 210 (2004) 105.
[8] J.L. Brito, F. Severino, N.N. Delgado, J. Laine, Appl. Catal. A: Gen. 173 (1998) 193.
[9] H. Nava, F. Pedraza, G. Alonso, Catal. Lett. 99 (2005) 65.
[10] R. Cattaneo, T. Weber, T. Shido, R. Prins, J. Catal. 191 (2000) 225.
[11] V. Sundaramurthy, A.K. Dalai, J. Adjaye, Catal. Lett. 102 (2005) 299.
[12] L. Coulier, G. Kishan, J.A.R. van Veen, J.W. Niemantsverdriet, J. Phys. Chem. B 106 (2002) 5897.
[13] M. Breysse, C. Geantet, P. Afanasiev, J. Blanchard, M. Vrinat, Catal. Today 130 (2008) 3.
[14] Z.-D. Huang, W. Bensch, L. Kienle, S. Fuentes, G. Alonso, C. Ornelas, Catal. Lett. 124 (2008) 24.
[15] G.M. Dhar, G.M. Kumaran, M. Kumar, K.S. Rawat, L.D. Sharma, B.D. Raju, K.S.R. Rao, Catal. Today 99 (2005) 309.
[16] L. Vradman, M.V. Landau, M. Herskowitz, V. Ezersky, M. Talianker, S. Nikitenko, Y. Koltypin, A. Gedanken, J. Catal. 213 (2003) 163.
[17] T. Klimova, L. Lizama, J.C. Amezcua, P. Roquero, E. Terrés, J. Navarrete, J.M. Domínguez, Catal. Today 98 (2004) 141.
[18] G.M. Kumaran, S. Garg, K. Soni, M. Kumar, L.D. Sharma, G.M. Dhar, K.S.R. Rao, Appl. Catal. A: Gen. 305 (2006) 123.
[19] O.Y. Gutiérrez, G.A. Fuentes, C. Salcedo, T. Klimova, Catal. Today 116 (2006) 485.
[20] O.Y. Gutiérrez, D. Valencia, G.A. Fuentes, T. Klimova, J. Catal. 249 (2007) 138.
[21] Z.-D. Huang, W. Bensch, L. Kienle, S. Fuentes, G. Alonso, C. Ornelas, Catal. Lett. 122 (2008) 57.
[22] Z.-D. Huang, W. Bensch, L. Kienle, S. Fuentes, G. Alonso, C. Ornelas, Catal. Lett. 127 (2008) 132.
[23] D.Y. Zhao, J.L. Feng, Q.S. Huo, N. Melosh, G.H. Fredrickson, B.F. Chmelka, G.D. Stucky, Science 279 (1998) 548.
[24] D.Y. Zhao, Q.S. Huo, J.L. Feng, B.F. Chmelka, G.D. Stucky, J. Am. Chem. Soc. 120 (1998) 6024.
[25] Z.-D. Huang, W. Bensch, W. Sigle, P.A. van Aken, L. Kienle, T. Vitova, H. Modrow, T. Ressler, J. Mater. Sci. 43 (2008) 244.
[26] M. Poisot, W. Bensch, S. Fuentes, G. Alonso, Thermochim. Acta 444 (2006) 35.
[27] L. Cambi, A. Cagnasso, A. Tanara, Atti Linc. 13 (1931) 404.
[28] D.D. Whitehurst, T. Isoda, I. Mochida, Adv. Catal. 42 (1998) 345.
[29] R. Candia, B.S. Clausen, H. Topsøe, J. Catal. 77 (1982) 564.
[30] M.V. Landau, L. Vradman, M. Herskowitz, Y. Koltypin, A. Gedanken, J. Catal. 201 (2001) 22.
[31] Y. Iwata, K. Sato, T. Yoneda, Y. Miki, Y. Sugimoto, A. Nishijima, H. Shimada, Catal. Today 45 (1998) 353.
[32] M. Poisot, W. Bensch, S. Fuentes, C. Ornelas, G. Alonso, Catal. Lett. 117 (2007) 43.
[33] E. Furimsky, F.E. Massoth, Catal. Today 17 (1993) 535.
[34] M. Absihalabi, A. Stanislaus, D.L. Trimm, Appl. Catal. 72 (1991) 193.

[35] R. Prada Silvy, P. Grange, F. Delannay, B. Delmon, Appl. Catal. 46 (1989) 113.
[36] W.H. Qian, Y. Hachiya, D.H. Wang, K. Hirabayashi, A. Ishihara, T. Kabe, H. Okazaki, M. Adachi, Appl. Catal. A: Gen. 227 (2002) 19.
[37] S. Eijsbouts, L.C.A. van den Oetelaar, R.R. van Puijenbroek, J. Catal. 229 (2005) 352.
[38] R.R. Chianelli, G. Berhault, Catal. Today 53 (1999) 357;
G. Berhault, A. Mehta, A.C. Pavel, J. Yang, L. Rendon, M.J. Yacaman, L.C. Araiza, A.D. Moller, R.R. Chianelli, J. Catal. 198 (2001) 9.
[39] C. Glasson, C. Geantet, M. Lacroix, F. Labruyere, P. Dufresne, J. Catal. 212 (2002) 76.
[40] G. Alonso, R.R. Chianelli, S. Fuentes, B. Torres, US Patent (2007) 7,223,713.
[41] M. Daage, R.R. Chianelli, J. Catal. 149 (1994) 414.